Journal of The Electrochemical Society, 2024 **171** 034505

Experimental Investigation of Naphthalene Induced Degradation of Reversible Solid Oxide Cells Operated on Bio-Syngas

B. Steinrücken,[1,z] S. Herrmann,[1] F. Kerscher,[1] K. Feigl,[1] A. Schwiers,[2,3] C. Lenser,[2] N. H. Menzler,[2,3] O. Guillon,[2,3] and H. Spliethoff[1]

[1]*Chair of Energy Systems, Technical University of Munich, Germany*
[2]*Inst. of Energy and Climate Research, IEK-1: Materials Synthesis and Processing, Forschungszentrum Jülich GmbH, Germany*
[3]*RWTH Aachen University, Institute of Mineral Engineering, Aachen, Germany*

The influence of the operational conditions and the electrode material on the degradation induced by the model tar naphthalene on 10 × 10 cm^2 fuel-electrode supported solid oxide cells operated on artificial bio-syngas under internal reforming conditions is experimentally investigated. Two different fuel electrodes are investigated based on yttrium-stabilized zirconia (YSZ) and gadolinium-doped ceria (GDC). A parameter study of the operational temperature and the operation mode (fuel cell or electrolysis mode) is conducted with the YSZ-based fuel electrode to quantify the effects on the cell degradation. The fuel off-gas composition and electrochemical impedance spectra are used to characterize the cell prior to the experiment and monitor its performance during the poisoning process. The influence of the tar on the Ni-YSZ electrode cell is investigated for an operation at 700 °C and 800 °C in fuel cell mode, and an operation at 700 °C in electrolysis mode. The experiment at 700 °C is repeated with the Ni-GDC electrode cell. At the increased operational temperature, the Ni-YSZ cell is more robust but carbon depositions occur. The voltage degradation during electrolysis operation increases significantly compared to fuel cell operation. The Ni-GDC electrode does not show an increased robustness compared to the Ni-YSZ electrode.
 [DOI: 10.1149/1945-7111/ad2cb9]

Manuscript submitted October 20, 2023; revised manuscript received December 31, 2023. Published March 7, 2024. *This paper is part of the JES Focus Issue on SOFC XVIII: Advances in Solid Oxide Fuel Cell and Electrolysis Cell Technology.*

The transformation towards a carbon-neutral society requires efficient and carbon-neutral power generation as well as highly efficient integration of renewable electricity for the decarbonization of the various sectors. A coupled biomass gasifier and solid oxide fuel cell (SOFC) plant enables highly efficient electrical power generation.[1] Integrating a solid oxide electrolyzer cell (SOEC) into a biomass gasification-based process, e.g., for generating sustainable aviation fuels, allows a highly efficient pathway to increase carbon utilization.[2] In both cases, the solid oxide cell (SOC) is at risk of carbon depositions and degradation. Equilibrium calculations can estimate the carbon deposition free operational area, which is usually visualized in ternary diagrams.[3] However, depositions and degradation effects of larger and especially polycyclic aromatic components, called tars in this work, cannot be predicted via this method.[4] The tars can either be catalytically reformed by the cell and used as fuel, block electrochemical active sites resulting in a degradation of the electrochemical performance without structural degradation, or form carbon depositions damaging the cell.[5,6] The standard approach to eliminate this risk is to use a gas cleaning unit, thus increasing the system complexity.[7] To avoid this step or to help define the requirements for the gas purity, several authors investigated the influence of aromatic compounds on SOFCs. The utilization of model tars tends to overestimate the influence of real tars[8] and is, therefore, a conservative approach commonly used. The most prominent utilized model tars are naphthalene,[9–18] toluene,[8,10–12,15,17–32] phenol[14,33] and benzene.[4,10,11,26,27,34,35] In comparative studies, naphthalene shows the lowest tendency to coke formation[11] and the highest impact on the catalytic methane reforming[12] as well as on the electrochemical performance.[10] Hence, it was chosen in this work to investigate the electrochemical degradation under internal reforming conditions.

Utilizing carbon-containing fuels derived from biomass gasification, the methane steam reforming reaction 1 and the water gas shift reaction 2 take place. Both reactions are catalyzed by the nickel in the cell and can be influenced by tars.

$$CH_4 + H_2O \rightleftharpoons 3H_2 + CO \quad [1]$$

$$CO + H_2O \rightleftharpoons H_2 + CO_2 \quad [2]$$

Naphthalene can be reformed similarly to methane at the catalytic active sites of the cell via (3).

$$C_{10}H_8 + 10H_2O \rightleftharpoons 10CO + 14H_2 \quad [3]$$

Fuel electrode supported single cells (FESCs) operated under internal reforming conditions between 700 °C and 750 °C show a fast voltage degradation during the exposure to naphthalene concentrations between 0.05 g Nm^{-3} and 0.4 g Nm^{-3}.[13,17,18] The operation under a H_2/N_2 mixture increases the robustness towards the tar, a stable operation at 0.3 g Nm^{-3} naphthalene is possible.[17] For a 2-cell stack operated under internal reforming conditions at 705 °C, a voltage degradation similar to the single cells is observed immediately at the start of the exposure to 2 g Nm^{-3} naphthalene. After 25 h the voltage degradation reaches a steady state. During the degradation the methane and CO off-gas concentration increases, whereas the H_2 and CO_2 concentrations decrease. The off-gas concentrations reach a steady state at the same time as the voltage.[14] In these investigations, Ni-YSZ electrodes and Ni-YSZ substrate layers are utilized and no carbon depositions are reported.[13,14,17,18]

In all investigated electrolyte supported cells (ESCs), Ni-GDC electrodes are used. For operations under internal reforming conditions between 830 °C and 900 °C, a voltage degradation under load is reported for naphthalene concentrations between 0.3 and 3.1 g Nm^{-3}.[12,15,36] For cells operated between 830 °C and 900 °C under internal reforming at open circuit conditions (OCC), an increase of the voltage is reported for tar concentrations of 3 and 11.6 g Nm^{-3}.[10,16] At OCC and under load an increase in the methane off-gas composition due to a degradation of the methane reforming is reported.[10,12,15,16] At a fully degraded state indicated by the steady state of the degraded voltage, 60% of the methane is still reformed.[15] For a H_2/N_2 gas mixture at 850 °C the open circuit voltage (OCV) increases and the 3 g Nm^{-3} naphthalene are partially reformed.[9] For the operation at 830 °C and 438 mA cm^{-2} under internal reforming conditions, an immediate voltage decrease with a stabilization within

[z]E-mail: benjamin.steinruecken@tum.de

the first hours is observed. The tar hinders the methane reforming and reversed water gas shift reaction with a more severe effect at higher concentrations. An area specific resistance increase is monitored, and after a recovery period of 24 h operation without tar dosing, the voltage has almost reached the value before the exposure.[36] No carbon deposition or metal dusting are reported for these experiments with naphthalene.[9,10,12,15,16,36]

Cells with a Ni-GDC fuel electrode are reported to be more robust towards carbon depositions than Ni-YSZ cells.[37] For naphthalene-induced degradation, the methane reforming reaction does not stop entirely and the voltage degradation occurs at higher tar concentrations compared to the Ni-YSZ electrode. This increased robustness is based on the mixed ionic conductor behavior of the GDC as well as the ability of ceria oxide to oxidize hydrocarbons.[38] This electrode is the standard material used in electrolyte-supported cells and was investigated via electrochemical impedance spectroscopy by several groups.[39,40] Due to the Ni-GDC electrode being solely utilized in ESCs, they are operated at a higher temperature compared to the Ni-YSZ electrode cells, limiting the comparability of the two electrode materials. Therefore, this work focuses on utilizing the Ni-GDC electrode on an FESC to compare both electrodes at the same operational conditions. Applying a Ni-GDC electrode on a Ni-YSZ fuel electrode-supported cell results in an interdiffusion of the ceria with an 8YSZ electrolyte forming Kirkendall voids. To avoid this issue, the utilization of a tri-layer electrolyte with a Gd-doped ceria barrier between the electrode and the electrolyte was proposed.[41] Recently, the first prototypes of this cell have been developed and tested.[42]

Reversible operation of solid oxide cells' can reduce their degradation under a regular operation without impurities.[43] Concerning the degradations induced by impurities in electrolyzer mode, the current research has not focused on tars yet. The effect of sulfur in the SOFC mode is similar compared to naphthalene. It is a potent poison for the electrochemical and catalytic performance, reducing the methane steam reforming and the water gas shift reaction. Hauch et al.[44] observed a sensitivity increase in orders of magnitude for Ni-YSZ FESCs operated at CO_2/CO electrolysis compared to SOFC operation at similar conditions explained by local carbon depositions for global test conditions outside the theoretically calculated range. In this work, the reported increased robustness of the Ni-GDC electrode is investigated in a FESC under internal reforming conditions with the model tar naphthalene. The operational temperature of the Ni-YSZ electrode reference cell is increased to ensure that the reported increased robustness of the ESCs is material and not temperature induced. The influence of the operational mode on the naphthalene induced degradation is investigated.

Experimental

The used cells are based on a tape-cast NiO (Vogler, The Netherlands) - $Y_{0.148}Zr_{0.852}O_{1.926}$ (8YSZ, UCM Advanced Ceramics, Laufenburg, Germany) support. The Ni-YSZ cells consist of functional screen-printed and sintered layers, which are applied in the following order:

a ~7 μm thick NiO-8YSZ fuel electrode layer

a ~10 μm thick 8YSZ electrolyte layer (8YSZ: Tosoh, Japan)

a ~7 μm thick $Gd_{0.2}Ce_{0.8}O_{2-\delta}$ (20GDC, Treibacher Industrie AG, Austria) air electrode barrier layer and a $La_{0.58}Sr_{0.4}Co_{0.2}Fe_{0.8}O_{3-\delta}$ (LSCF) air electrode layer (LSCF: synthesized in house by spray drying and calcination).

The Ni-GDC cells consist of functional layers in the following order and, if not mentioned otherwise, are applied by screen-printing and sintering:

a ~10 μm thick NiO-GDC fuel electrode layer

a ~5 μm thick 10GDC (fuelcellmaterials, USA) electrolyte layer

a ~600 nm thick 8YSZ electron blocking layer applied by physical vapor deposition (PVD)

a ~500 nm thick 20GDC air electrode barrier layer applied by PVD

Table I. Operational parameters of the syngas operation with current density *i*, fuel utilization *FU* and tar dry gas concentration $c_{Naph,dry}$.

Param.	Value	
H_2	0.25 Nl min^{-1}	25 vol%
H_2O	0.50 Nl min^{-1}	50 vol%
CO_2	0.10 Nl min^{-1}	10 vol%
CO	0.10 Nl min^{-1}	10 vol%
CH_4	0.05 Nl min^{-1}	5 vol%
i	± 0.34 A cm^{-2}	
FU	0.3	
$c_{Naph.,dry}$	0.4 g Nm^{-3}	

and a $La_{0.6}Sr_{0.4}CoO_{3-\delta}$ (LSC) air electrode layer (LSC: synthesized in house as LSCF). The half-cells of the Ni-YSZ cells are sintered at 1400 °C, the barrier layer at 1300 °C, and the LSCF layer at 1080 °C. The detailed process is described elsewhere.[45] For the Ni-GDC electrode FESC, the process by Zhang et al.[42] is used. All screen-printing pastes were synthesized by mixing the ceramic powder with terpineol to form a pre-suspension, then adding a transport agent consisting of ethyl cellulose dissolved in terpineol. Screen printing was performed on a semi-automatic screen printer (X1, EKRA, Germany). The Ni-GDC might be prone to gas leakage and/or electronic leakage currents since the 10GDC electrolyte shows some defects that might originate from a non-ideal electrolyte paste or substrate inhomogeneities. These defects might not be covered entirely by the thin PVD layers. It should be mentioned that these cells are still under development and not as mature as the cells with YSZ electrolyte.

The cells are characterized by the single-cell test bench (Evaluator C1000-HT with TrueData-Load V3 and TrueData-EIS, Horiba FuelCon, Germany) detailed elsewhere.[33,46] The fuel gases H_2, CO, CO_2, N_2, and CH_4 are dosed via its mass flow controllers, and steam is added via the thermally controlled bubbler. A full ceramic housing is used, with a 72 cm^2 gold mesh at the air side and two nickel meshes at the fuel side. The tar is dosed via a thermally controlled evaporator pot flushed with the CO_2 gas stream as carrier gas. A description of the dosage unit[6] and the concentration calculation[14] is detailed elsewhere. The tar dosage is occasionally validated with a solid phase adsorption method, described by Fischer et al.[47] The anode off-gas composition is measured via a gas analysis (GENTWO Multigas, M&C TechGroup, Germany) utilizing a thermal conductivity detector for 0–100 vol% H_2 and a nondispersive infrared sensor for 0–30 vol% CO, 0–70 vol% CO_2 and 0–10 vol% CH_4. Before the gas analysis, the gas is cleaned via a compressor gas cooler (ECM-1, M&C TechGroup, Germany) at 5 °C and a separator. To ensure the required minimum gas flow in the gas analysis of 1.2 Nl min^{-1}, a membrane pump recirculates the gas flow through the gas analysis. The flow is manually controlled via two needle valves regulating the recirculation flow over two bypasses: one over the pump and one over the pump and the gas analysis. The operational conditions of the cell can be found in Table I. The gas composition is shown in the ternary diagram in Fig. 1; the boundaries for carbon deposition are calculated with FactSage™ for graphite. The influence of the tar on the C-H-O composition is neglected due to its insignificant concentration. No carbon depositions are expected from the operational conditions.

The tar-induced degradation of a reference Ni-YSZ cell at 700 °C is compared to the degradation at 800 °C, a Ni-GDC cell at 700 °C and the electrolysis operation of a Ni-YSZ cell at 700 °C by the measured cell voltage and electrochemical impedance spectroscopy (EIS) data. Ten spectra each decade are measured between 0.1 Hz and 10 kHz. Wherever possible, the recommendations of Klotz et al.[48] are followed for the measurements. The data points of the EIS measurement with a positive imaginary part, due to inductive effects in the set-up, are removed. The

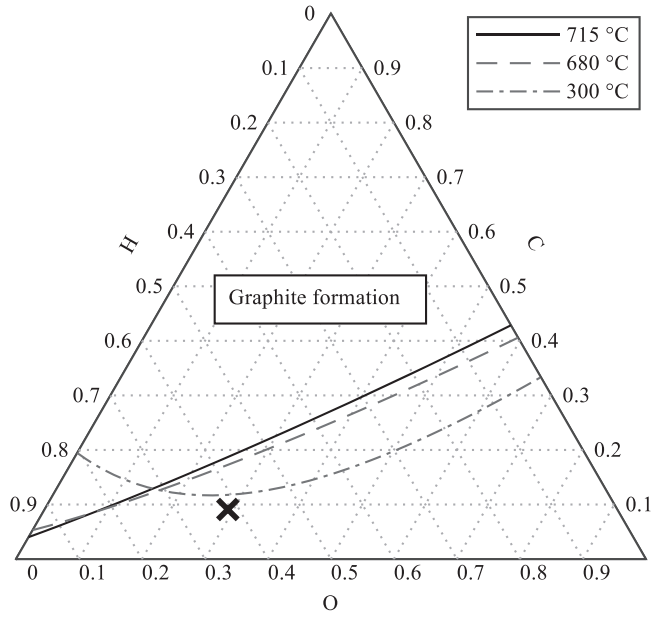

Figure 1. Ternary diagram for the risk of carbon depositions calculated for graphite; the operational point in this work without the tar is marked.

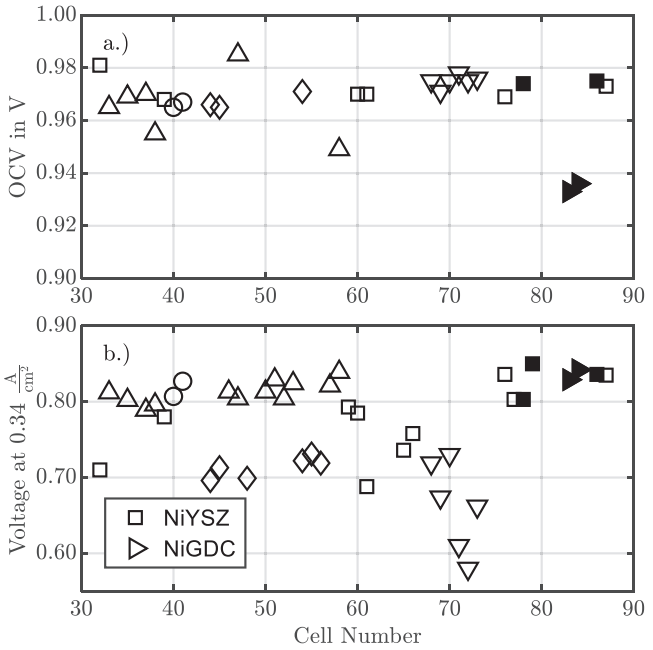

Figure 2. Comparison of the cells investigated in this work (solid symbols) with past results[6] (open symbols) at 700 °C for syngas operation at 0.34 A cm^{-2} in (a) and OCC in (b).

distribution of relaxation times (DRT) analysis is performed by an in-house tool based on the FTIKREG Tool by Weese et al.[49] A starting value of the regularization parameter is determined by the L-curve curvature criteria similar to the procedure of Choi et al.[50] It is kept within a narrow interval for related measurement series.

Results

Before the degradation experiments, the cells are characterized with clean syngas (no tar dosing) to ensure a correct assembly and to gain a first understanding of the impedance spectra of the Ni-GDC electrode cells.

Cell characterization.—The cell's performances at open circuit conditions under syngas operation are shown in Fig. 2a in comparison to past FESCs results[6] in chronological order, different symbols are indicating different cell types. An average performance of the Ni-YSZ cells is observed with open circuit voltages of around 0.975 V. The spread is due to slightly different gas tightness and a difference in the temperature and humidity by the combustion of leaking hydrogen. The Ni-GDC cells show a drastically reduced OCV due to insufficient gas tightness of the electrolyte. The voltages at 0.34 A cm^{-2} are shown in Fig. 2b. The cells are all performing on a similar level, between 0.80 V and 0.85 V. The voltage of the Ni-GDC cells is equal to the Ni-YSZ cells. Hence, the Ni-GDC cells compensate for their reduced gas tightness with an improved performance. The long-term trend of the cells in Fig. 2 towards better performance is explained by stepwise improvement of the setup and procedure.

To further verify the setup and the cell's performance, the operation at the reference operational conditions is compared to the results of a 0D simulation via the model proposed by Hauck et al.,[50] which can be found in Table II. In addition, the exhaust gas compositions are added to this table. While the voltage of all cells is sufficiently similar compared to the simulation results, the gas composition varies significantly. Although a leakage of air into the gas analysis due to the recirculation is compensated for the shown data, the hydrogen content for all cells is significantly lower than calculated. This is probably induced by a combustion due to the air leakage in the setup and the housing.

To investigate the novel Ni-GDC fuel electrode, a temperature variation is conducted between 680 and 750 °C. The measured

Table II. Comparison of the normalized fuel off-gas compositions of the investigated cells with the simulated results for syngas operation.

Exp. Name	Sim.	700 °C	800 °C	Ni-GDC	SOEC
V at 0.34 A cm^{-2}	0.807 V	0.803 V	0.850 V	0.829 V	0.836 V
H_2 in vol%	55.5	45.5	30.2	41.0	43.3
CO in vol%	11.8	13.4	30.6	12.4	13.4
CO_2 in vol%	32.5	41.1	39.0	46.5	43.4
CH_4 in vol%	0.0	0.0	0.3	0.0	0.0
N_2 in vol%	0	0	0	0	0

electrochemical impedance spectra and the calculated distributions of relaxation times are shown in Fig. 3. The ohmic resistance decreases with an increased temperature due to the increased ionic conductivity of the electrolyte with rising temperatures. The polarization resistance declines with increasing temperatures. The temperature change only slightly affects the low frequency arc, whereas the high frequency arc is the main driving force of the observed changes. The DRT identifies four different processes. The first one at 1 Hz increases with a rising temperature, whereas the processes at 20 Hz and 300 Hz decrease. The temperature does not affect the last identified process at around 1500 Hz. Reliable identification of all four processes requires vast data points and is complicated by gradients over the 10 × 10 cm^2 cell. Since it is known that the chemical capacity of the ceria electrode overlaps with the gas diffusion impedance of the cell,[39] the peak at 1 Hz is assumed to be related to both chemical capacitance and mass transfer process at the fuel electrode due to the internal reforming conditions. The peaks at 20 Hz and 300 Hz are assumed to be related to the electrochemical reaction in the fuel electrode, since the impedance of the LSC air electrode is likely too small to be visible in the spectra.[42]

Standard operation.—The off-gas composition *y* for the Ni-YSZ cell operated under syngas at 700 °C is shown in Fig. 4. At t = 0 h, the dosage of naphthalene is started. There were some technical

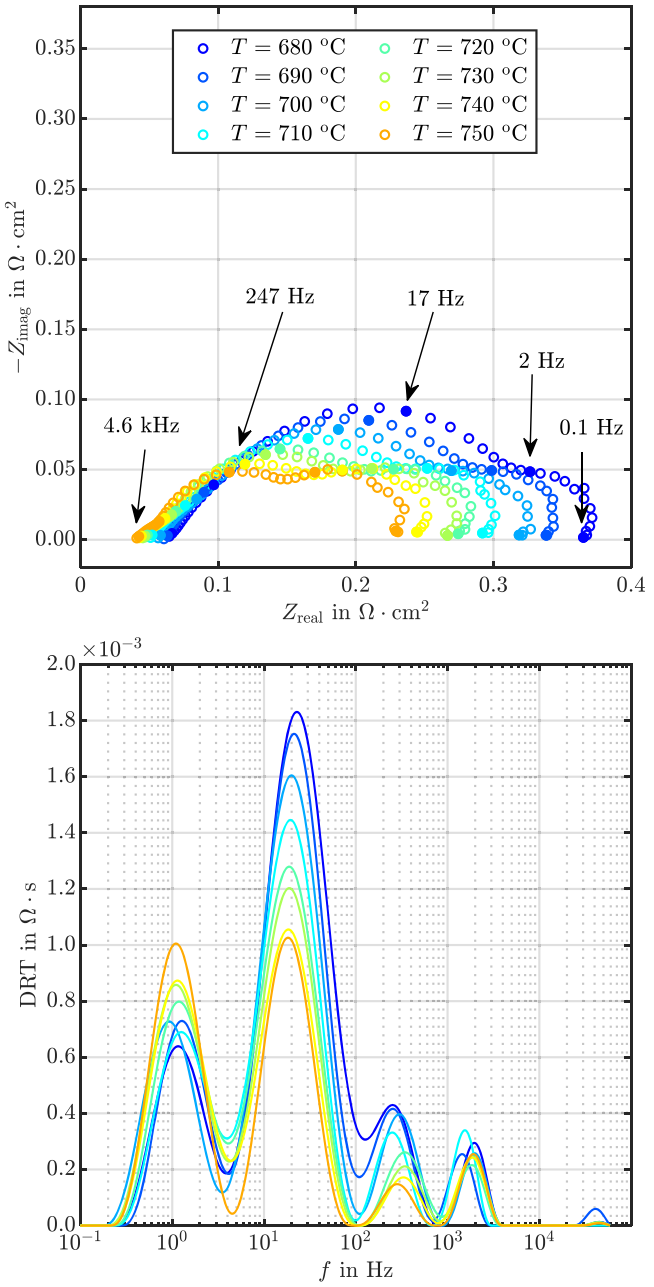

Figure 3. EIS and DRT of the Temperature variation of the Ni-GDC FESC operated under syngas conditions.

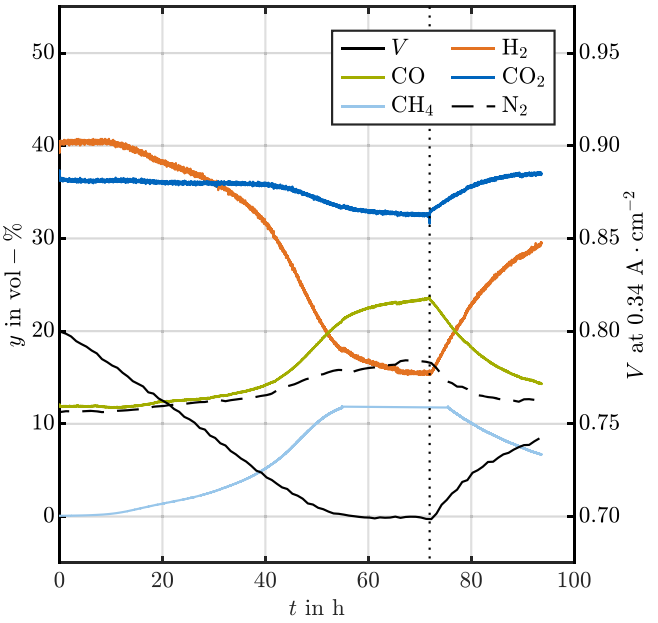

Figure 4. Influence of 0.4 g Nm^{-3} naphthalene on the off-gas composition and voltage of the Ni-YSZ cell operated at 700 °C under 0.34 A cm^{-2}.

issues at the start of the degradation experiment of the reference cell. Hence, it's likely that the start point of the dosage is shifted to t = −1…−2 h. Shortly after the dosage started, a degradation of the voltage begins. The voltage degradation stops at around 100 mV after approximately 50 h. A minor regeneration occurs until the end of the naphthalene dosage marked with the dashed line. The off-gas composition is affected by naphthalene as well. The methane reformation gets poisoned, similar to the voltage degradation. The steady state is reached at approximately 50 h, outside the sensor's measurement range. This voltage and off-gas composition degradation is similar to the results observed for a short stack operated under the same gas composition at 2 g Nm^{-3} naphthalene.[14] The tar does not affect the cell's ohmic resistance, as shown in Fig. 5. The polarization resistance continuously increases up to 60 h of poisoning, with both arcs growing. This is in line with the observations of prior experiments.[13] In the DRT, all four processes are affected, with a focus on the first two. The process at the highest frequency has a high risk of being an artifact due to the limited measured frequencies up to 10 kHz. No indications of carbon depositions were found in the cell operated at 700 °C.

Elevated operational temperature.—For an operational temperature of 800 °C, the naphthalene-induced degradation of the voltage and off-gas compositions is shown in Fig. 6.

Due to the temperature increase, the degradation is reduced compared to the standard operation. The behavior of the voltage is similar to the 700 °C operation, with a degradation for 50 h and a steady state operation until the end of the tar dosage. However, the voltage degradation with a magnitude of 50 mV is half the value of the reference operation. In the off-gas composition, the methane reforming is only slightly reduced with a maximum methane off-gas composition of 1.4 vol%. After the dosage, the methane reforming is completely regenerated within a few hours. The fluctuations in the gas compositions are due to the low gas tightness of the assembly and pressure fluctuations due to a day-night shift. The electrochemical impedance spectra at elevated temperature are less prone to degradation, as shown in Fig. 7.

The change in the polarization resistance is only minor compared to the operation at 700 °C. The DRT shows that the tar no longer affects the fuel conversion resistance at 1 Hz. This is assumed to result from the reduced influence of the tar on the methane reforming. Only the peak at 300 Hz is affected by the tar but on a lower magnitude compared to the degradation of this process at 700 °C. The degradation in this process shows a blockage of the active site at the fuel electrode or a decrease in the fuel transport to the electrode. Massive carbon depositions were found in an optical post-mortem analysis, as shown in Fig. 8. The solid depositions are detected in the flowfield, as well as at the mesh, the cell, and the gold wires.

For FESCs operated at internal reforming conditions with naphthalene no carbon depositions were reported for temperatures up to 750 °C.[18] With Ni-GDC ESCs, a carbon deposition-free operation at internal reforming conditions with temperatures of up to 900 °C and tar concentrations of up to 11.6 g Nm^{-3} is reported.[16] The ESCs operated at comparable temperatures lack the Ni-YSZ substrate layer, which is more vulnerable to depositions than the Ni-GDC electrode.

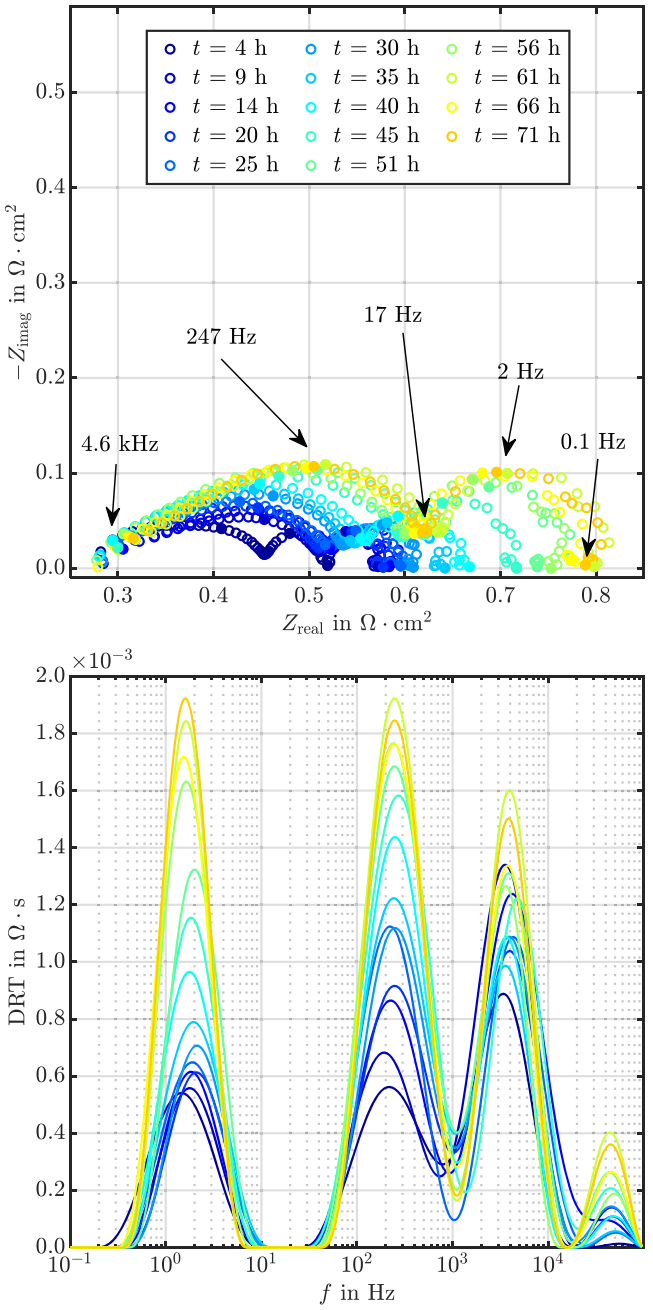

Figure 5. Influence of 0.4 g Nm^{-3} naphthalene on the impedance spectra and DRT of the Ni-YSZ cell operated at 700 °C under 0.34 A cm^{-2}.

Experimental investigation of the set-up.—To separate the influence of the cell from the set-up, the operation at 800 °C was repeated with a gas tight Crofer 22 APU steel sheet instead of a cell. For a more realistic comparison, a current of 0.34 A cm^{-2} was used via the electric power supply. The off-gas composition is shown in Fig. 9.

The nickel mesh reforms a portion of the methane to around 8%. The reforming process is poisoned by the tar and partially regenerates as well. At the fully degraded state, the CO and CO_2 content are identical; no water gas shift reaction occurs. The behavior is similar but accelerated to the observed cell off-gas composition, explained by the reduced number of catalytic active centers of the Ni-mesh compared to the cell. The steady state is reached after 0.5 h, and the regeneration is completed after 1.5 h. Compared to the observed timeframes of the cell (50 h degradation), the influence of the Ni-mesh can be neglected. A minor amount of

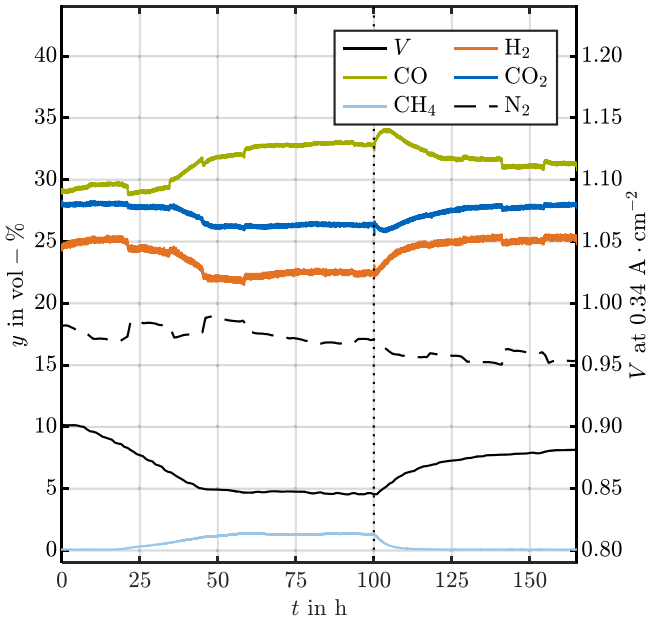

Figure 6. Influence of 0.4 g Nm^{-3} naphthalene on the off-gas composition and voltage of the Ni-YSZ cell operated at 800 °C under 0.34 A cm^{-2}.

carbon depositions was detected at the gold wires inside the housing. These depositions are assumed to be either thermally induced or artifacts from the previous experiment. Due to the usage of a current of 24.3 A, the gold wires are heating up. The tar molecules can thermally decompose, resulting in local carbon depositions. The experiment was repeated without a current, and no traces of carbon deposition were detected. Hence, the observed depositions in the experiments conducted with an FESC are catalyzed by the Ni in the cell. It is assumed that the substrate layer is the origin of these depositions due to the lack of available O^{2-} ions, a lower steam concentration in the substrate pores compared to the electrode, and its larger active area due to its porous structure and thickness.

Investigation of the Ni-GDC electrode.—In comparison to the Ni-YSZ cells, the Ni-GDC cell voltage and off-gas composition is shown in Fig. 10 for an operation with naphthalene dosing at 700 °C.

Both cells perform similarly when poisoned with the tar. The voltage degradation is nearly identical, but the off-gas composition varies slightly. This variation is probably induced by differences in the assembly and the gas tightness. Therefore, the assumption that the mixed conductor electrode is more robust towards naphthalene degradation could not be proven. Due to the low gas tightness of the electrolyte, this result needs to be reproduced with improved cells before any final conclusion can be made. In this experiment, no indication of carbon deposition was found. Burn marks on the air electrode of the Ni-GDC cell indicated pores in the electrolyte. The evolution of the EIS and DRT during the degradation is shown in Fig. 11.

The tar heavily influences the impedance spectra. The dominating process is the increase of the polarization resistance; the ohmic resistance increases slightly. The growth of the polarization resistance from 0.2 $\Omega\,\mathrm{cm}^{-2}$ to 0.6 $\Omega\,\mathrm{cm}^{-2}$ is large enough to offset the prior better performance of the Ni-GDC electrode compared to the Ni-YSZ. In the direct comparison of the evolution during the degradation process of the normalized ohmic and polarization resistance in Fig. 12, the Ni-GDC cell exhibits a different behavior from the Ni-YSZ cells.

For both Ni-YSZ cells, the evolution is similar, with an increase of the polarization resistance to around 1.5 and a slightly declining ohmic resistance dominated by noise. For the Ni-GDC cell, the ohmic resistance increases to 1.5 and the polarization resistance to 2.2. The slopes of all trends are similar, but the magnitude is

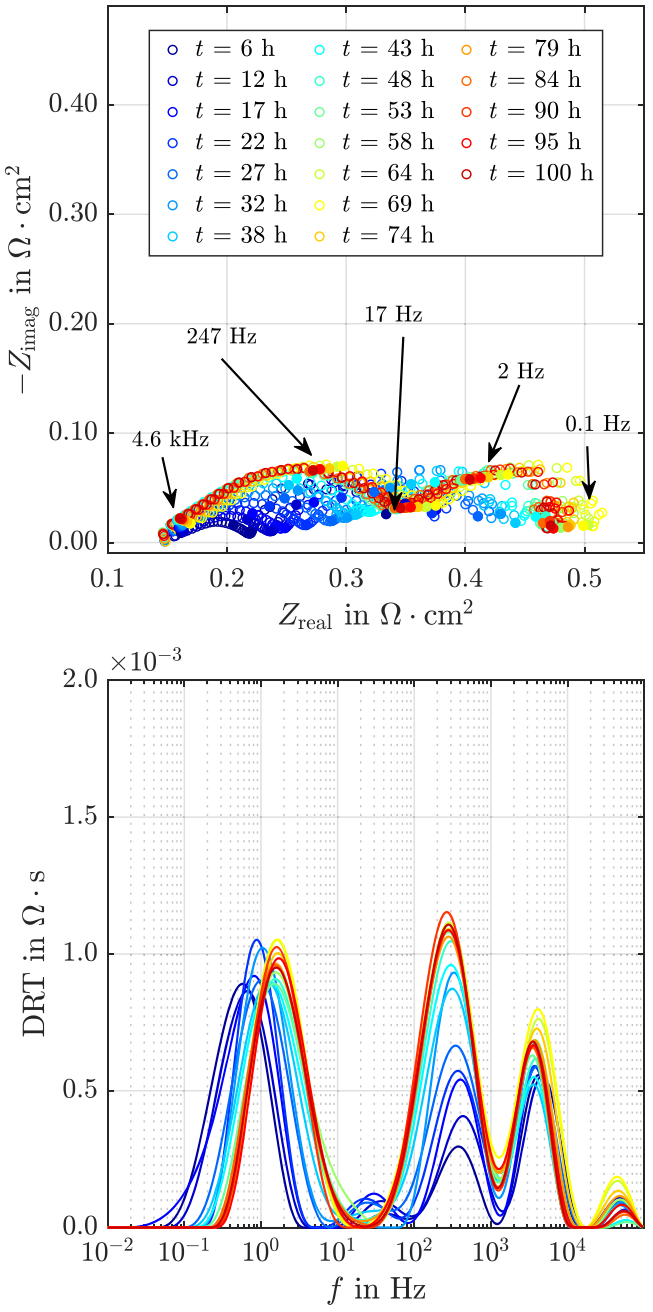

Figure 7. Influence of 0.4 g Nm^{-3} naphthalene on the impedance spectra and DRT of the Ni-YSZ cell operated at 800 °C under 0.34 A cm^{-2}.

increased. During the regeneration after the tar dosage, the ohmic resistance only partially regenerates. This indicates a superimposing of two different processes, a permanent and a non-permanent one resulting in the observed degradation of the ohmic resistance. The main origin of the ohmic resistance is the limited ionic conduction. Increasing the diffusion length results in an increased ohmic resistance. A possible reason for the increase in the pathway length is an increase in the thickness of the electrochemical active layer, possibly due to the partially reversible tar blockage of electrochemical active centers. The increased size of the electrochemical active layer can exceed the thickness of the Ni-GDC electrode. The DRT in Fig. 11 shows that the increase of the first peak (fuel reforming process) is the main driving force of the degradation. The process at 20 Hz is only slightly influenced by the degradation. The change in the last two processes is within the range of the uncertainties. Hence, compared to the Ni-YSZ cell, the degradation is mainly driven by

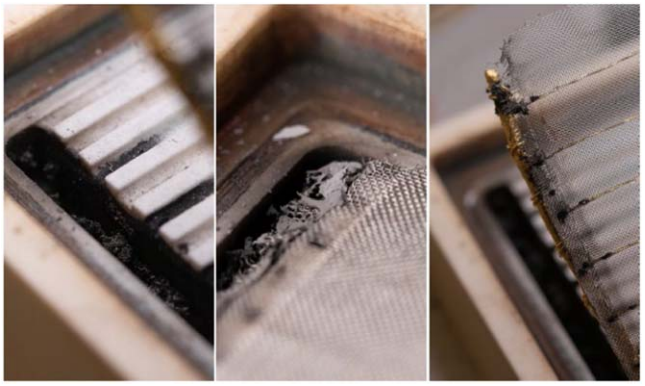

Figure 8. Pictures of the carbon depositions detected for the Ni-YSZ cell operated at 800 °C under syngas conditions.

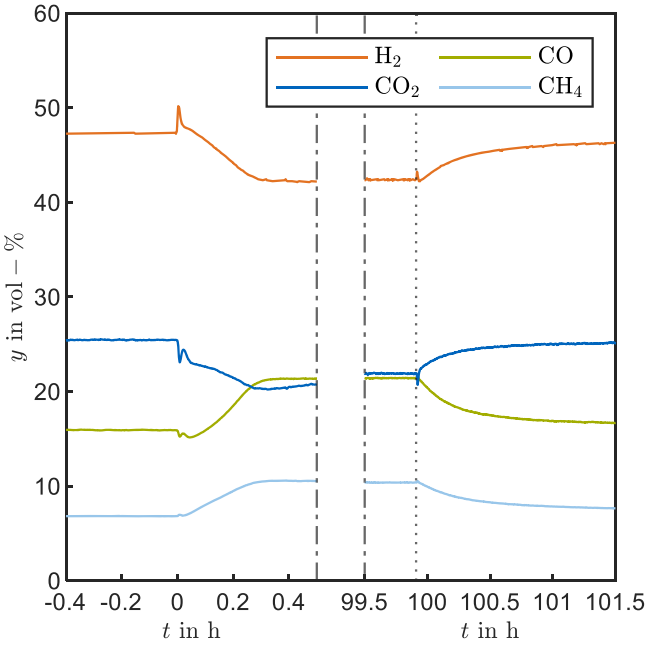

Figure 9. Fuel off-gas analysis for the naphthalene poisoning of the set-up with a Crofer 22 APU steel sheet instead of a cell at 800 °C under syngas conditions.

the first process. It is assumed that the poisoning of the methane reforming in the substrate is the main driving force of this increase. Therefore, the robustness towards naphthalene is unaffected by an improved electrode material.

SOEC operation.—The voltage of the Ni-YSZ cell operated in electrolysis mode is shown in Fig. 13. It is far more vulnerable towards the naphthalene-induced degradation than the SOFC operation. The maximum voltage degradation of 250 mV is reached after around 50 h. Afterwards, a slight recovery is observed. The absolute voltage degradation is increased from 0.1 V at SOFC operation to 0.25 V at SOEC operation. The maximum methane content is around 6.8%, instead of above 12.5% observed in the SOFC mode. The electrolysis mode consumes water and produces hydrogen, increasing the dry gas flow and decreasing the concentrations of all gasses besides hydrogen. Utilizing the 0D Modell, a methane off-gas concentration without internal reforming of 7.4% is calculated. The deviation from the model is within the uncertainties. Hence, a complete inhibition of the methane reforming reaction is assumed. Due to the degradation of the steam methane reforming it is no longer consuming water. This is affecting the water gas shift reaction, inverting its direction. The change of the shift's direction

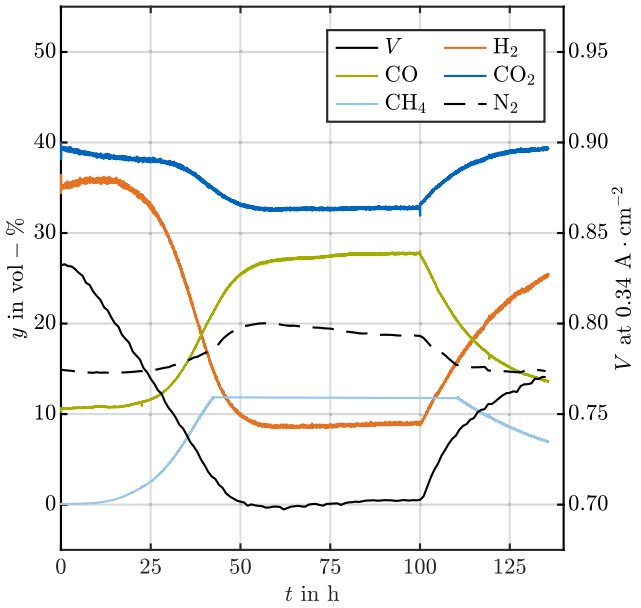

Figure 10. Influence of 0.4 g Nm^{-3} naphthalene on the off-gas composition and voltage of the Ni-GDC electrode cell operated at 700 °C under 0.34 A cm^{-2}.

is visible in the CO and CO_2 concentrations. After around 40 h, the CO_2 concentration exceeds the CO concentration. Due to the inhibition of the methane reforming, the increased water fraction is expected to reduce the voltage at operational conditions and at OCC, similar to the reduced voltage observed in the SOFC experiments. The opposite effect is observed for the SOEC mode; the voltage increases drastically.

The i-V curves before and after the poisoning are plotted in Fig. 14. The curve was recorded at the end of the shown regeneration process. The i-V curve after the degradation is strongly non-linear. The influence of the tar on the voltage in the SOEC regime is more potent than in the SOFC regime. At the SOFC regime, the behavior of the degraded cell is in the range of prior results. At the standard operation of 0.34 A cm^{-2}, the voltage difference is around 70 mV, similar to the other cells in this work. The OCV is slightly reduced compared to the reference due to the increased water content. The voltage difference between the reference and the degraded cell in SOEC mode is up to a magnitude of 2.5 larger than the SOFC degradation. This effect on the voltage is even more severe if the increased steam content and reduced OCV are considered. Additionally, the i-V curve, recorded starting at SOEC operation after the degradation, shows a hysteresis. This phenomenon can be induced by electrochemical oxidation of some adsorbed naphthalene at the triple phase boundaries (TPB) during the SOFC mode. During the SOFC mode, the available O^{2-}-ions at the TPB are potentially supporting the decomposition of the adsorbed tar resulting in a short blockage period of the TPB by the tar. Additionally, the steam produced by the electrochemical reaction is locally improving the tar reformation as well. In the SOEC mode, there are no O^{2-}-ions available to support the decomposition at the TPB and the steam concentration required for the chemical reforming reaction is locally, and globally, reduced by the TPB. Hence, the tar reformation at the TPB is inhibited by the operational mode.

Discussion

At the elevated temperature of 800 °C, the voltage and methane reforming degradations are reduced compared to the standard operation at 700 °C. Severe carbon depositions disable a stable operation for an industrial-relevant duration. Without the cell, close to no depositions are occurring. A comparison of the observed carbon depositions at elevated temperature with literature results

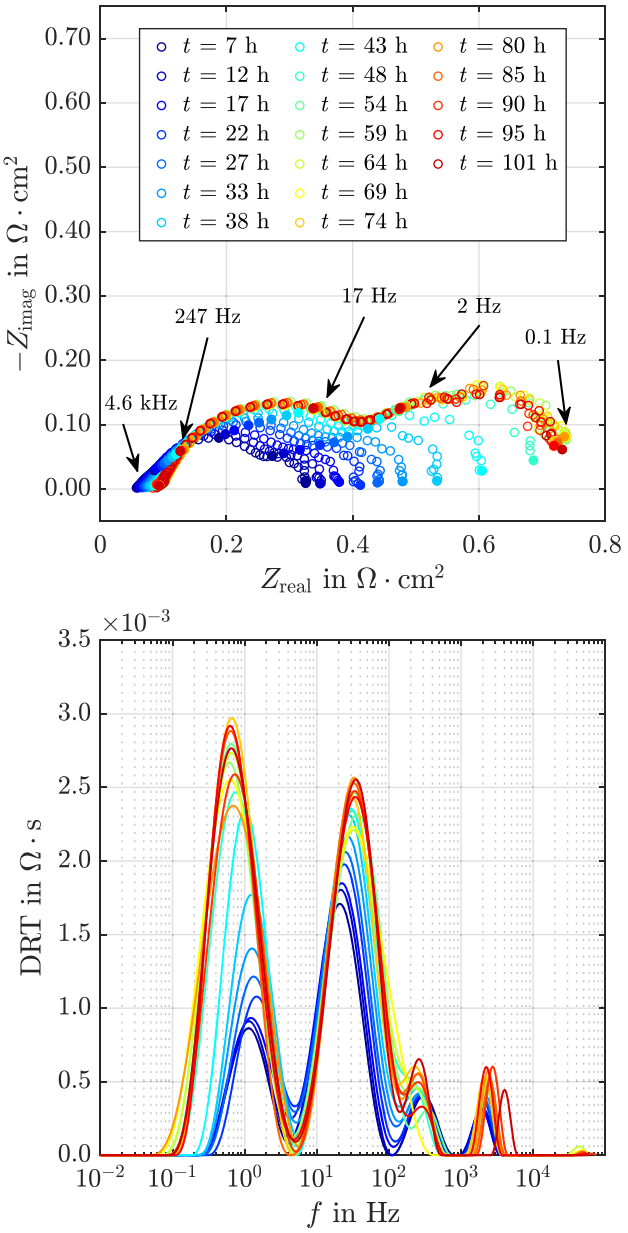

Figure 11. Influence of 0.4 g Nm^{-3} naphthalene on the impedance spectra and DRT of the Ni-GDC electrode cell operated at 700 °C under 0.34 A cm^{-2}.

shows that the operational conditions, temperature, gas compositions, and fuel side materials influence the risk of depositions. A general transfer of results with other materials or gas compositions is not possible.

Utilizing the Ni-GDC electrode in the fuel electrode supported cell did not increase the robustness towards naphthalene. In the DRT of these novel cells, four different processes are shown under internal reforming conditions. During the naphthalene-induced degradation, the decisive process is the first at 1 Hz. For similar FESC with a Ni-YSZ electrode, the process at 1 Hz is associated with the diffusion of CO/CO_2[51] and is further amplified by an internal reforming reaction.[52] Its growth is assumed to be induced by the tar-induced degradation of the internal methane reforming in the Ni-YSZ substrate. Hence, for internal reforming conditions, the influence of the contaminant on the Ni-YSZ substrate is as crucial as its influence on the electrode. The ohmic resistance of the Ni-GDC cell is heavily increased by the tar as compared to the Ni-YSZ cells. This degradation is only partially reversible indicating the

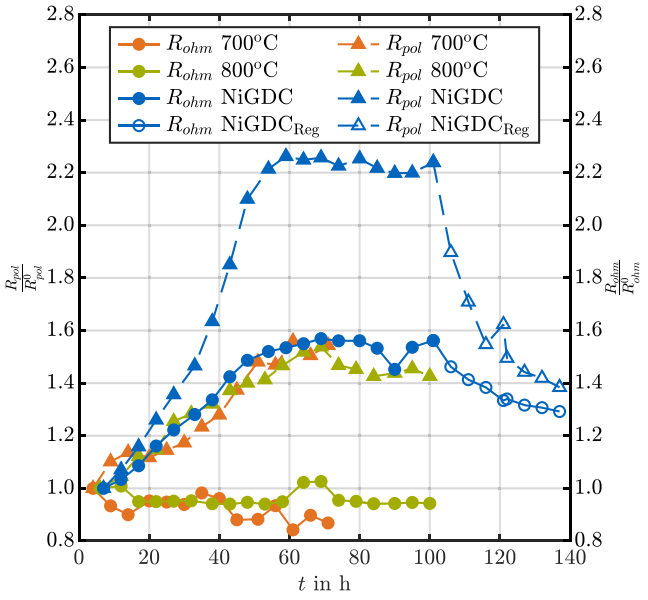

Figure 12. Evolution of the normalized polarization and ohmic resistances during the poisoning process and the regeneration of the Ni-GDC cell.

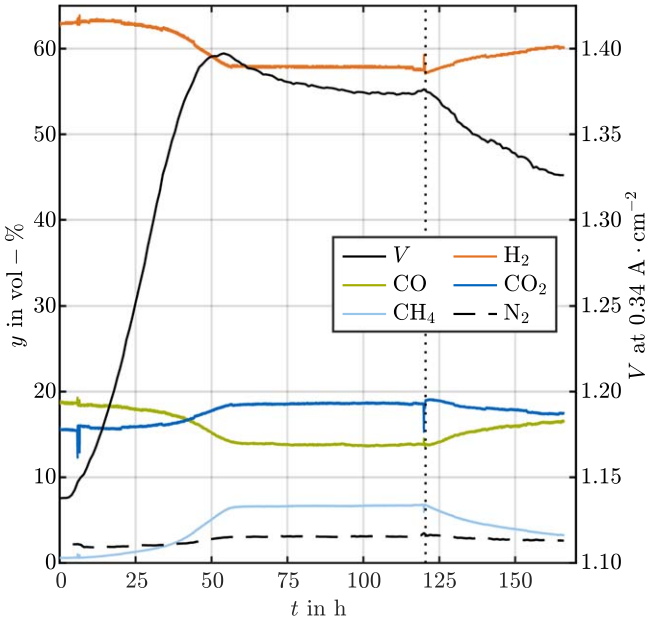

Figure 13. Influence of 0.4 g Nm^{-3} naphthalene on the off-gas composition and voltage of the Ni-YSZ cell operated at 700 °C under −0.34 A cm^{-2}.

superimposing of an irreversible and a reversible process. During the regeneration after the tar dosage, electrochemical sites blocked by the tar are expected to regenerate due to the decomposition of the tar. A partial delamination of the electrode-electrolyte interface, a crack formation within the electrolyte, interface effects between the three layers of the electrolyte as well as other irreversible processes due to the cell being a prototype are possible explanations for the observed permanent degradation of the ohmic resistance.

For both experiments with the Ni-YSZ and the Ni-GDC cell in the SOFC mode at 700 °C, an increase in the CO concentration and a decrease in the CO_2 concentration is measured. This indicates a decline in the water gas shift reaction with both concentrations approaching each other. In the SOEC mode, this trend increases, and the water gas shift reaction is reversed, resulting in a higher CO than CO_2 concentration. Compared with the SOFC operation, the influence of the tar on the hydrogen content is low. This can be

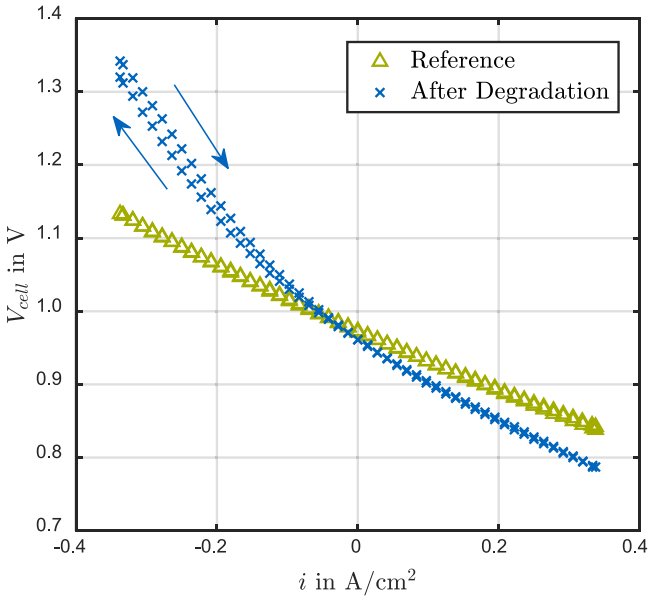

Figure 14. i-V curves of the Ni-YSZ cell operated at 700 °C before (reference) and after the degradation and a short recovery time.

only partially explained by the increased total dry flow and, thereby, decreased ratio of the reformed hydrogen from the total measured hydrogen flow. Nevertheless, due to the stoichiometric ratio in the steam methane reforming, a higher impact of its degradation on the hydrogen concentration was expected.

The voltage in electrolysis operation shows a 2.5-fold increased degradation compared to the fuel cell mode. The cell voltage in the SOFC regime aligns with the other results in this work. Due to this operational mode-dependent voltage degradation, a permanent degradation due to carbon depositions can be ruled out. The proposed theory for this behavior is an inhibited reforming of the tar at the TPB due to the lack of O^{2-}-ions as well as the decreased steam concentration compared to the SOFC mode. A possible different approach to explain the observed behavior is the influence of the tar on the water gas shift reaction, resulting in unfavorable mass transport conditions in the substrate layer, resulting in a hindered transport of the water to the electrochemically active sites. Further investigations and reproducing the results are necessary to fully prove these theories.

The comparison of all investigated cells at the standard operational condition syngas at 700 °C shows a deviation in the voltage and off-gas composition. Several systematic sources for these uncertainties have been identified: An aging of the gold seal occurs over the experiments. The assembly is conducted manually; the positioning of the cell, meshes, sealings, and voltage sense wires will vary in each setup. The ambient pressure in the laboratory fluctuates in a day-night cycle and is further influenced by the building's ventilation. The used cells are manufactured manually. Therefore, the systematic uncertainties dominate the statistical ones by the used equipment. The starting point of each degradation experiment is used as reference to eliminate the influence of the systematic uncertainties. The tar concentration is chosen to induce a degradation effect that is sufficiently larger than the uncertainties. Compared with reference data,[13] the standard operation of the Ni-YSZ cell reproduced similar results for the voltage and the EIS, validating the setup and method.

Similar experiments for a naphthalene-induced degradation of the Ni-YSZ fuel electrode cells at similar operational conditions have not reported a structural degradation for cell and stack experiments.[13,14,17,18] Hence, no post-mortem analysis for the operation at 700 °C was conducted. The depositions at 800 °C were severe and visible without further investigations.

Conclusions

The influence of the operational conditions and the electrode material on the degradation induced by the model tar naphthalene on fuel-electrode supported solid oxide cells operated on artificial biosyngas is investigated. The electrolysis mode is observed to be more vulnerable to poisoning by the selected tar than the fuel cell mode. The available results did not enable a final explanation for this phenomenon. Further investigations are thus required. The poisoning effects, whether a performance degradation or carbon deposition, depend not only on the type of tar but also on the operational conditions and the fuel side materials. The influence of the substrate layer is crucial. Hence, a more detailed investigation of this layer is necessary. The FESC with Ni-GDC fuel-electrode did not show the expected higher robustness. This investigated cell is a prototype and a more detailed investigation is required when the development is finished.

Acknowledgments

The investigations in the fuel cell operation mode have been supported by the Deutsche Forschungsgemeinschaft (DFG) within the project SynSOFC II (SP 367/5–2), the investigations of the electrolysis operation mode have been endorsed by the Federal Ministry of Education and Research (BMBF) within the project REDEFINE H2E (01DD21005). Both are gratefully acknowledged.

ORCID

B. Steinrücken https://orcid.org/0000-0001-6797-6225
F. Kerscher https://orcid.org/0000-0002-1450-6032
A. Schwiers https://orcid.org/0000-0002-2825-3574
C. Lenser https://orcid.org/0000-0001-5636-2201
N. H. Menzler https://orcid.org/0000-0001-7091-0980

References

1. Z. Wu, P. Zhu, J. Yao, S. Zhang, J. Ren, F. Yang, and Z. Zhang, *Appl. Energy*, **279**, 115794 (2020).
2. B. Steinrücken, M. Dossow, M. Schmid, M. Hauck, S. Fendt, F. Kerscher, H. Spliethoff, and J. R. Smith, *36th International Conference on Efficiency, Cost, Optimization, Simulation and Environmental Impact of Energy Systems (ECOS 2023)* (ECOS, Las Palmas De Gran Canaria, Spain) p. 1170 (2023) 10.52202/069564-0107.
3. K. Sasaki, *Proc. Vol.*, **2003-07**, 1225 (2003).
4. J. Mermelstein, M. Millan, and N. P. Brandon, *J. Power Sources*, **196**, 5027 (2011).
5. Z. Ud Din and Z. A. Zainal, *Renew. Sustain. Energy Rev.*, **72**, 1050 (2017).
6. M. Hauser, *Effects of Tars on Solid Oxide Fuel Cells, München, Dr Hut* (2021).
7. P. V. Aravind and W. de Jong, *Prog. Energy Combust. Sci.*, **38**, 737 (2012).
8. E. Lorente, M. Millan, and N. P. Brandon, *Int. J. Hydrogen Energy*, **37**, 7271 (2012).
9. P. V. Aravind, J. P. Ouweltjes, N. Woudstra, and G. Rietveld, *Electrochem. Solid-State Lett.*, **11**, B24 (2008).
10. A. Cavalli and P. V. Aravind, *ECS Trans.*, **91**, 781 (2019).
11. R. Coll, J. Salvadó, X. Farriol, and D. Montané, *Fuel Process. Technol.*, **74**, 19 (2001).
12. N. J. J. Dekker, J. P. P. Ouweltjes, and B. Rietveld, *ECS Trans.*, **7**, 1465 (2007).
13. M. Hauser, S. Herrmann, M. Hauck, S. Fendt, H. Jeong, C. Lenser, N. H. Menzler, and H. Spliethoff, *ECS Trans.*, **91**, 697 (2019).
14. M. Hauser, S. Herrmann, M. Hauck, S. Fendt, C. Lenser, N. H. Menzler, and H. Spliethoff, *J. Electrochem. Soc.*, **167**, 124514 (2020).
15. M. Hauth, T. Kienberger, and J. Karl, *ECS Trans.*, **35**, 2713 (2011).
16. M. Hauth, W. Lerch, K. König, and J. Karl, *J. Power Sources*, **196**, 7144 (2011).
17. D. Papurello, A. Lanzini, D. Drago, P. Leone, and M. Santarelli, *Energy*, **95**, 67 (2016).
18. D. Papurello, A. Lanzini, P. Leone, and M. Santarelli, *Renewable Energy*, **2016**, 747 (2016).
19. A. Baldinelli, G. Cinti, U. Desideri, and F. Fantozzi, *Energy Convers. Manage.*, **128**, 361 (2016).
20. P. Boldrin, M. Millan-Agorio, and N. P. Brandon, *Energy Fuels*, **29**, 442 (2015).
21. A. Cavalli, M. Kunze, and P. V. Aravind, *Appl. Energy*, **231**, 1 (2018).
22. T. S. Doyle, Z. Dehouche, P. V. Aravind, M. Liu, and S. Stankovic, *Int. J. Hydrogen Energy*, **39**, 12083 (2014).
23. M. Liu, M. G. Millan, P. V. Aravind, and N. Brandon, *J. Electrochem. Soc.*, **158**, B1310 (2011).
24. M. Liu, A. van der Kleij, A. Verkooijen, and P. V. Aravind, *Appl. Energy*, **108**, 149 (2013).
25. H. Madi, S. Diethelm, C. Ludwig, and J. van herle, *ECS Trans.*, **68**, 2811 (2015).
26. J. Mermelstein, M. Millan, and N. P. Brandon, *Chem. Eng. Sci.*, **64**, 492 (2009).
27. J. Mermelstein, M. Millan-Agorio, and N. Brandon, *ECS Trans.*, **17**, 111 (2009).
28. T. Namioka, Y. Nagai, K. Yoshikawa, and T. Min, *Int. J. Hydrogen Energy*, **37**, 17245 (2012).
29. T. Namioka, T. Naruse, and R. Yamane, *Int. J. Hydrogen Energy*, **36**, 5581 (2011).
30. D. Papurello, V. Chiodo, S. Maisano, A. Lanzini, and M. Santarelli, *Renewable Energy*, **127**, 481 (2018).
31. D. Papurello, C. Iafrate, A. Lanzini, and M. Santarelli, *Appl. Energy*, **208**, 637 (2017).
32. D. Pumiglia, S. Vaccaro, A. Masi, S. J. McPhail, M. Falconieri, S. Gagliardi, L. Della Seta, and M. Carlini, *J. Power Sources*, **340**, 150 (2017).
33. M. Hauser, S. Herrmann, S. Fendt, H. Jeong, C. Lenser, N. H. Menzler, and H. Spliethoff, *Int. J. Hydrogen Energy*, **43**, 20417 (2018).
34. J. Mermelstein, N. Brandon, and M. Millan, *Energy Fuels*, **23**, 5042 (2009).
35. J. Mermelstein, M. Millan, and N. Brandon, *J. Power Sources*, **195**, 1657 (2010).
36. A. Cavalli and P. V. Aravind, *Int. J. Hydrogen Energy*, **46**, 21124 (2021).
37. E. Lorente, C. Berrueco, M. Millan, and N. P. Brandon, *J. Power Sources*, **242**, 824 (2013).
38. M. J. Escudero, I. Gómez de Parada, A. Fuerte, and J. L. Serrano, *J. Power Sources*, **253**, 64 (2014).
39. C. Grosselindemann, N. Russner, S. Dierickx, F. Wankmüller, and A. Weber, *J. Electrochem. Soc.*, **168**, 124506 (2021).
40. A. Hagen, A. K. Padinjarethil, and J. Heijne, *Electrochim. Acta*, **461**, 142672 (2023).
41. A. Schwiers, C. Lenser, O. Guillon, and N. H. Menzler, *J. Eur. Ceram. Soc.*, **43**, 6189 (2023).
42. J. Zhang, C. Lenser, N. Russner, A. Weber, N. H. Menzler, and O. Guillon, *J. Am. Ceram. Soc.*, **106**, 93 (2023).
43. C. Graves, S. D. Ebbesen, S. H. Jensen, S. B. Simonsen, and M. B. Mogensen, *Nat. Mater.*, **14**, 239 (2015).
44. A. Hauch, M. L. Traulsen, R. Küngas, and T. L. Skafte, *J. Power Sources*, **506**, 230108 (2021).
45. W. Schafbauer, N. H. Menzler, and H. P. Buchkremer, *Int J Applied Ceramic Tech*, **11**, 125 (2014).
46. B. Steinrücken, S. Herrmann, M. Hauck, and H. Spliethoff, *ECS Trans.*, **103**, 1817 (2021).
47. F. Fischer, M. Hauser, M. Hauck, S. Herrmann, S. Fendt, H. Jeong, C. Lenser, N. H. Menzler, and H. Spliethoff, *Energy Sci. Eng.*, **40**, 270 (2019).
48. D. Klotz, A. Weber, and E. Ivers-Tiffée, *Electrochim. Acta*, **227**, 110 (2017).
49. J. Weese, *Comput. Phys. Commun.*, **1992**, 99 (1992).
50. M. Hauck, S. Herrmann, and H. Spliethoff, *Int. J. Hydrogen Energy*, **42**, 10329 (2017).
51. A. Kromp, *Model-Based Interpretation of The Performance and Degradation of Reformate Fueled Solid Oxide Fuel Cells* (2013).
52. P. Caliandro, A. Nakajo, S. Diethelm, and J. van herle, *J. Power Sources*, **436**, 226838 (2019).